



Cite this: *RSC Adv.*, 2016, 6, 94976

Catalytic aerobic oxidation of 5-hydroxymethylfurfural into 2,5-diformylfuran over VO^{2+} and Cu^{2+} immobilized on amino-functionalized core-shell magnetic $\text{Fe}_3\text{O}_4@ \text{SiO}_2$

Longfei Liao, Ying Liu,* Zengyong Li, Junping Zhuang, Yanbin Zhou and Size Chen

Amino modified $\text{Fe}_3\text{O}_4@ \text{SiO}_2$ ($\text{Fe}_3\text{O}_4@ \text{SiO}_2\text{-NH}_2$) was used to immobilize Cu^{2+} and VO^{2+} for preparing $\text{Fe}_3\text{O}_4@ \text{SiO}_2\text{-NH}_2\text{-Cu}^{2+}$ and $\text{Fe}_3\text{O}_4@ \text{SiO}_2\text{-NH}_2\text{-VO}^{2+}$ catalysts. Various technologies had been used for the characteristics of catalysts, such as XRD, XPS, FT-IR, SEM, TEM and VSM. The catalytic performance of $\text{Fe}_3\text{O}_4@ \text{SiO}_2\text{-NH}_2\text{-VO}^{2+}$ in HMF oxidation could be significantly enhanced by the use of $\text{Fe}_3\text{O}_4@ \text{SiO}_2\text{-NH}_2\text{-Cu}^{2+}$ as the co-catalysts. The type of reaction solvents showed a great influence on the oxidation of HMF. The highest HMF conversion reached up to 98.7% at 110 °C in toluene with an optimal 2,5-diformylfuran yield of 85.5%. Moreover, the $\text{Fe}_3\text{O}_4@ \text{SiO}_2\text{-NH}_2\text{-Cu}^{2+}$ and $\text{Fe}_3\text{O}_4@ \text{SiO}_2\text{-NH}_2\text{-VO}^{2+}$ catalyst exhibited great stability and could be readily applied in the next recycle after magnetic separation.

Received 14th July 2016
Accepted 27th September 2016

DOI: 10.1039/c6ra17932k

www.rsc.org/advances

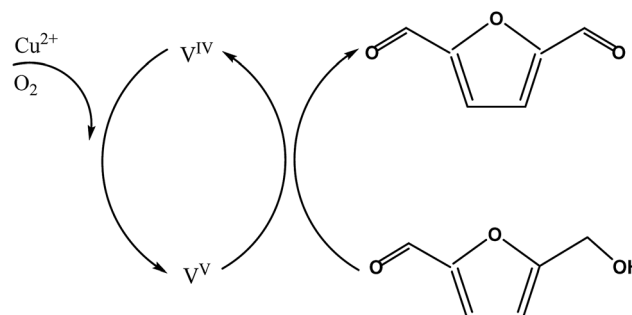
1. Introduction

With gradually diminishing fossil fuel reserves, great efforts are now being made worldwide to convert renewable biomass into fuels and value-added chemicals.¹⁻⁵ The oxidation of 5-hydroxymethylfurfural (HMF) is of great industrial importance owing to the extensive use in pharmacy and chemical industry.⁶⁻⁸ Among high-valued potential chemicals, DFF is applied to furanic polymers,⁹ a precursor for pharmaceuticals and antifungal agents,^{10,11} and a renewable furan-urea resin.¹² Moreover, DFF is also known as a promising alternative to petroleum-based terephthalic acid since its poor solubility in most organic solvents which renders its applications.¹³

In recent years, a series of homogeneous and heterogeneous catalysts have been studied for the oxidation of HMF. In the process of homogeneous catalysts, the oxidation of HMF with oxygen molecule using a mixed Co/Mn/Zr/Br system had been conducted and DFF attained a yield of 57.0%.¹⁴ However, recycling these homogeneous catalysts is rather difficult. As a result, different heterogeneous catalysts have been studied toward the selective aerobic oxidation of HMF including silver-containing manganese meso-porous molecular sieves, polymer-supported IBX-amide,¹⁵ Mn(m)-salen complex¹⁶ and Ru/hydroxalcite catalysts.¹⁷ However, the whole process of recycling heterogeneous catalysts by centrifugation and/or filtration is generally time-consuming. Interestingly, magnetic separation is environmentally

friendly, simple and considered to be more effective than common methods.^{18,19} It is believed that $\text{Fe}_3\text{O}_4@ \text{SiO}_2\text{-NH}_2\text{-VO}^{2+}/\text{Cu}^{2+}$ catalytic system may promote the HMF oxidation by the $\text{V}^{\text{IV}}/\text{V}^{\text{V}}$ redox cycle of vanadium, which means the V^{IV} species of vanadium was oxidized to V^{V} species by the co-promotion of molecular oxygen and Cu^{2+} , since Cu^{2+} has strong oxidization, after that the V^{V} species of vanadium oxidize HMF into DFF, as shown by the following illustration (Scheme 1).

Magnetic microspheres, a major member of core-shell structured nanocomposites,²⁰⁻²² are used for magnetic separation. The amino-functionalization was one of the most common methods for the modification of magnetic microspheres, for example 3-aminopropyltriethoxysilane (APTES) was used to generate terminal amino groups ($-\text{NH}_2$) and form covalent bonds on the surface of the modified material. So far, considerable efforts have been done to graft amino groups on the



Scheme 1 The proposed redox cycle of oxidation of HMF catalyzed by $\text{Fe}_3\text{O}_4@ \text{SiO}_2\text{-NH}_2\text{-VO}^{2+}/\text{Cu}^{2+}$.

State Key Laboratory of Pulp and Paper Engineering, South China University of Technology, Guangzhou 510640, China. E-mail: amyliu@scut.edu.cn; Tel: +86 02022236719

surface of mesoporous silicas like SBA-15, MCM-41, HSM, and so forth.^{23–27} Recently, Zhang and his teammates have synthesized one type of amino-functionalized magnetic catalyst $\text{Fe}_3\text{O}_4@\text{SiO}_2\text{-NH}_2\text{-Ru(III)}$, which consists of Ru(III) supported on surface-modified Fe_3O_4 magnetite nanoparticles.²⁸ The magnetic catalysts exhibited great catalytic performance and can be well separated and easily recycled. More recently, Ma and coworkers reported that $\text{Cu}(\text{NO}_3)_2$ in combination with VOSO_4 demonstrated good catalytic activity in the oxidizing HMF into DFF.¹⁷ Furthermore, Liu reported that amino-modified SBA-15 (SBA-NH_2) was used to graft VO^{2+} and Cu^{2+} on the surface of SBA-15 with the highest HMF conversion $\sim 98.9\%$ at 110°C in 4-chlorotoluene.²⁹

The excellent catalytic activity of the homogeneous $[\text{Cu}(\text{NO}_3)_2\text{-VOSO}_4]$ catalysts inspired us to design a novel type of solid catalyst which contains anchored VO^{2+} and Cu^{2+} ions. In addition, since the high affinity of amino-modified $\text{Fe}_3\text{O}_4@\text{SiO}_2$ to transition metal cations, in this work, amino-modified silica-coated magnetic $\text{Fe}_3\text{O}_4@\text{SiO}_2$ was prepared to anchor Cu^{2+} and VO^{2+} for the HMF oxidation reaction with oxygen molecule. The effects of different reaction conditions on catalysts performance were discussed in details as well. These studies probably provide a viable method for industrial application of magnetic catalysts in the oxidative conversion of HMF.

2. Experimental

2.1. Materials

Tetraethoxysilane (TEOS, 99.6%), 3-aminopropyltriethoxysilane (98.0%) and vanadyl sulfate (VOSO_4) were purchased from Aladdin Industrial Corporation Co. Ltd. (Shanghai, China). $\text{FeCl}_3\cdot 6\text{H}_2\text{O}$ (99.5%), and $\text{FeSO}_4\cdot 7\text{H}_2\text{O}$ (99.5%) were purchased from Sinopharm Chemical Reagent Co., Ltd. (Shanghai, China). 5-Hydroxymethylfurfural (98.0%) and 2,5-diformylfuran (98.0%) were supplied by Tokyo Chemical Industry Co. Ltd. (Tokyo, Japan). 5-Hydroxymethyl-2-furoic acid (FFCA) was purchased from Adamas Co. Ltd. (Shanghai, China). All the solvents were purchased from Aladdin Chemicals Co. Ltd. (Shanghai, China) and freshly distilled before use. Acetonitrile (HPLC grade) was obtained from RCI Labscan Co. Ltd. (UK).

2.2. Catalyst preparation

Firstly, silica-coated Fe_3O_4 nanoparticles ($\text{Fe}_3\text{O}_4@\text{SiO}_2$) were used as magnetic supports, which were prepared and characterized according to the literature.³⁰ Briefly, Fe_3O_4 nanoparticles were prepared by the coprecipitation of ferrous and ferric salts with strong alkaline solution. Thereafter, Fe_3O_4 was coated with silica layers from TEOS as silica source to form $\text{Fe}_3\text{O}_4@\text{SiO}_2$ under alkaline conditions. $\text{Fe}_3\text{O}_4@\text{SiO}_2$ was further modified with APTES in dry toluene under N_2 atmosphere at the reflux temperature 110°C for 24 h. Then, the amino-modified solid (denoted as $\text{Fe}_3\text{O}_4@\text{SiO}_2\text{-NH}_2$) was separated by an external magnet and washed with toluene to eliminate residual APTES. At last, $\text{Fe}_3\text{O}_4@\text{SiO}_2\text{-NH}_2$ was dried at 80°C in a vacuum oven overnight.

2.3. Preparation of $\text{Fe}_3\text{O}_4@\text{SiO}_2\text{-NH}_2$ supported VO^{2+} and Cu^{2+}

The immobilization of VO^{2+} on $\text{Fe}_3\text{O}_4@\text{SiO}_2\text{-NH}_2$ was realized by the treatment of $\text{Fe}_3\text{O}_4@\text{SiO}_2\text{-NH}_2$ with VOSO_4 alcoholic solution. Typically, VOSO_4 (0.5 g) and $\text{Fe}_3\text{O}_4@\text{SiO}_2\text{-NH}_2$ (1.0 g) were added into 50 mL methanol and stirred at 70°C for 24 h. Then, the pale green mixture was well separated from the solution by an external magnet, washed with ethanol three times, centrifuged at the rotate rate of 9000 rpm, and then Soxhlet extracted with ethanol for 12 h for the removal of the residual vanadyl species. At last, the prepared catalysts were dried at 60°C in a vacuum oven overnight (denoted as $\text{Fe}_3\text{O}_4@\text{SiO}_2\text{-NH}_2\text{-VO}^{2+}$). A similar process was conducted in the preparation of $\text{Fe}_3\text{O}_4@\text{SiO}_2\text{-NH}_2\text{-Cu}^{2+}$ by $\text{Cu}(\text{NO}_3)_2$ (0.5 g) and $\text{Fe}_3\text{O}_4@\text{SiO}_2\text{-NH}_2$ (1.0 g).

2.4. Catalyst characterization

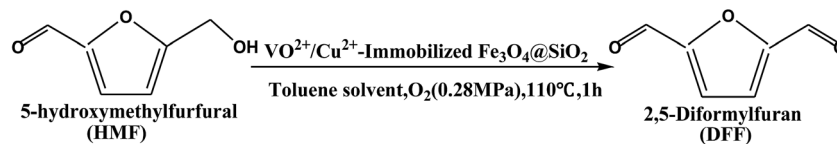
The morphology and structure of the catalysts were characterized by scanning electron microscopy (SEM, JEOL 2100F) and transmission electron microscope (TEM, Merlin). FT-IR measurements were determined with a VERTEX 33 FTIR spectrometer with the spectral resolution of 4 cm^{-1} in the wave number range of $4500\text{--}4000\text{ cm}^{-1}$. X-ray photoelectron spectroscopy (XPS) was conducted on a Thermo VG Scientific ESCA MultiLab-2000 spectrometer with a monochromatized Al K α source (1486.6 eV) at a constant analyzer pass energy of 25 eV. The binding energy was estimated to be accurate within 0.2 eV. All binding energies (BEs) were corrected referencing to the C 1s (284.6 eV) peak of the contamination carbon as an internal standard. X-ray powder diffraction (XRD) patterns of samples were performed on a Bruker Advance D8 powder diffractometer (Cu K α). Magnetization measurement was checked out by a Physical Property Measurement System (PPMS-9T) with VSM option from Quantum Design. The applied magnetic fields H between -30 and 30 kOe , the temperature was kept at 300 K .

2.5. Procedures of aerobic oxidation of HMF into DFF

The general scheme of aerobic oxidation of HMF into DFF is described in Scheme 2. All the reactions were conducted in an autoclave reactor volume of 100 mL. Typically, HMF (100 mg, 0.8 mmol), toluene (40 mL), $\text{Fe}_3\text{O}_4@\text{SiO}_2\text{-NH}_2\text{-VO}^{2+}$ (100 mg) and $\text{Fe}_3\text{O}_4@\text{SiO}_2\text{-NH}_2\text{-Cu}^{2+}$ (30 mg), were added and the autoclave reactor was flushed with O_2 for three times. Pressurized with O_2 again and heated up to the expected temperature, the operating oxygen pressure was maintained at 0.28 MPa (unless otherwise mentioned); all the reactions were conducted for 1 h with 650 rpm stirring. Finally, after all the reactions, the autoclave reactor was cooled to room temperature and the samples were analyzed with HPLC.

2.6. Analytical methods

The analysis of HMF and DFF was carried out on Alliance 2695 HPLC system. The products were well separated by a reversed-phase C18 column ($200 \times 4.6\text{ mm}$), and the detection wavelength was 284 nm. The mobile phase was constituted of 0.1



Scheme 2 The oxidation of HMF into DFF.

wt% trifluoroacetic acid and acetonitrile aqueous solution ($v : v = 70 : 30$) at 0.8 mL min^{-1} . The column temperature maintained at 25°C . The contents of DFF and HMF in the samples were calculated by the external standard calibration curve method, which were based on the pure compounds.

$$\text{HMF conversion} = \frac{\text{mol of converted HMF}}{\text{mol of starting DFF}} \times 100\%$$

$$\text{DFF yield} = \frac{\text{mol of DFF produced}}{\text{mol of starting HMF}} \times 100\%$$

2.7. Recycling of the catalysts

After all the reactions, the $\text{Fe}_3\text{O}_4@\text{SiO}_2\text{-NH}_2\text{-VO}^{2+}$ and $\text{Fe}_3\text{O}_4@\text{SiO}_2\text{-NH}_2\text{-Cu}^{2+}$ catalysts were well separated from the mixture by an external magnet, washed 3 times by ethanol, and dried in a vacuum oven at 60°C overnight. The collected catalysts were reused for the next cycle under the identical reaction conditions.

3. Results and discussion

3.1. Catalyst preparation and characterization

The Scheme 3 shows the general procedure for preparation magnetic catalysts. $\text{Fe}_3\text{O}_4@\text{SiO}_2$ was prepared and characterized according to the literature.³⁰ Then $\text{Fe}_3\text{O}_4@\text{SiO}_2$ was functionalized with 3-aminopropyl groups ($-\text{NH}_2$) by APTES in dry toluene under N_2 at 110°C for 24 h. The $\text{Fe}_3\text{O}_4@\text{SiO}_2\text{-NH}_2\text{-Cu}^{2+}$ and $\text{Fe}_3\text{O}_4@\text{SiO}_2\text{-NH}_2\text{-VO}^{2+}$ catalysts were prepared by the grafting of Cu^{2+} and VO^{2+} from $\text{Cu}(\text{NO}_3)_2$ and VOSO_4 aqueous solution with $\text{Fe}_3\text{O}_4@\text{SiO}_2\text{-NH}_2$, respectively. Throughout the

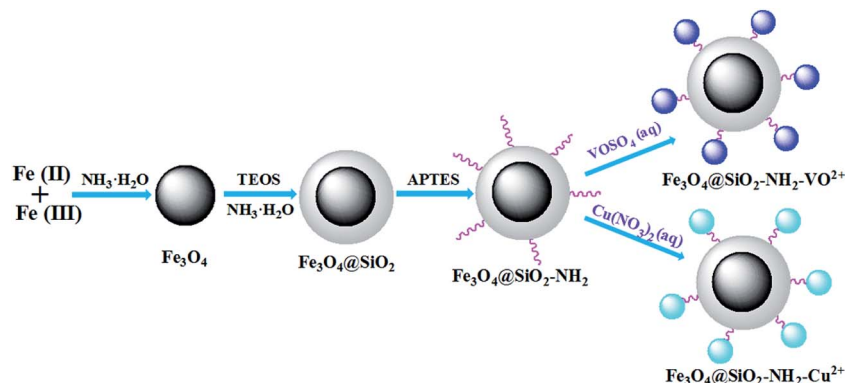
whole reaction process, the mixed black solution gradually became clear, which implied that $\text{Fe}_3\text{O}_4@\text{SiO}_2\text{-NH}_2$ grafted VO^{2+} . Similarly, the blue solution turned to be lighter, which also indicated that the loading of vanadium in the catalyst $\text{Fe}_3\text{O}_4@\text{SiO}_2\text{-NH}_2\text{-VO}^{2+}$ was designed to be 2.05 mmol g^{-1} . With the identical preparing conditions for $\text{Fe}_3\text{O}_4@\text{SiO}_2\text{-NH}_2\text{-VO}^{2+}$, the non-functionalized support $\text{Fe}_3\text{O}_4@\text{SiO}_2$ was also treated with VOSO_4 aqueous solution and the loading content of V was 0.06 mmol g^{-1} . Similarly, the loading of cuprum in the catalyst $\text{Fe}_3\text{O}_4@\text{SiO}_2\text{-NH}_2\text{-Cu}^{2+}$ was designed to be 1.77 mmol g^{-1} and the non-functionalized support $\text{Fe}_3\text{O}_4@\text{SiO}_2$ was also treated with $\text{Cu}(\text{NO}_3)_2$ aqueous solution and the loading content of Cu was 0.04 mmol g^{-1} .

The XRD diffraction patterns of (a) $\text{Fe}_3\text{O}_4@\text{SiO}_2\text{-NH}_2$, (b) $\text{Fe}_3\text{O}_4@\text{SiO}_2\text{-NH}_2\text{-Cu}^{2+}$ and (c) $\text{Fe}_3\text{O}_4@\text{SiO}_2\text{-NH}_2\text{-VO}^{2+}$ are shown in Fig. 1. There existed no apparent difference in the XRD patterns of three samples. The XRD peaks of the three samples were distributed to the planes of the inverse cubic spinel structure, which were consistent with the standard sample of Fe_3O_4 .^{30–32}

The SEM image of Fig. 2 also shows that the diameter of the microspheres is $\sim 100 \text{ nm}$, which is much larger than that of Fe_3O_4 due to SiO_2 successfully coated Fe_3O_4 nanoparticles. In addition, Fig. 2a and b show that the catalysts were well dispersed in the terms of morphology.

As showed in Fig. 2, the TEM image of $\text{Fe}_3\text{O}_4@\text{SiO}_2\text{-NH}_2\text{-Cu}^{2+}$ and $\text{Fe}_3\text{O}_4@\text{SiO}_2\text{-NH}_2\text{-VO}^{2+}$ microspheres (Fig. 3a) shows a typical core-shell structure. There is no difference between the two samples, the ions had been successfully grafted by NH_2 to the surface of the microspheres.

We further investigated the element distribution of $\text{Fe}_3\text{O}_4@\text{SiO}_2@m\text{SiO}_2\text{-NH}_2\text{-PW}$ by EDX. Fig. 4a and e show a STEM image of the catalyst, from which the sandwich-like core-shell

Scheme 3 The schematic illustration of the synthesis of $\text{Fe}_3\text{O}_4@\text{SiO}_2\text{-NH}_2\text{-Cu}^{2+}$ and $\text{Fe}_3\text{O}_4@\text{SiO}_2\text{-NH}_2\text{-VO}^{2+}$.

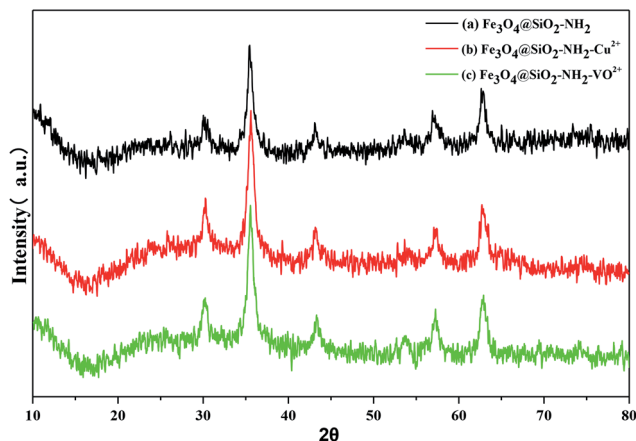


Fig. 1 XRD spectra of (a) $\text{Fe}_3\text{O}_4@\text{SiO}_2\text{-NH}_2$, (b) $\text{Fe}_3\text{O}_4@\text{SiO}_2\text{-NH}_2\text{-Cu}^{2+}$ and (c) $\text{Fe}_3\text{O}_4@\text{SiO}_2\text{-NH}_2\text{-VO}^{2+}$.

structure is clearly observed. Fig. 4b–d and f–h show the corresponding EDX mapping images collected from a single microsphere in the catalyst, confirming the existence of elements Fe, and Si. From the element distribution images, we can see that Fe enriched area is concentrated in the core area, and Si enriched area is mainly distributed in the inner and outer shells, which can confirm the existence of the $\text{Fe}_3\text{O}_4@\text{SiO}_2$ support. In the meantime, the distribution of Cu and V shows that both of the two elements are well dispersed in the microsphere. Therefore, we believe that Cu^{2+} and VO^{2+} are successfully anchored to the amino-functionalized $\text{Fe}_3\text{O}_4@\text{SiO}_2$.

The surface composition of $\text{Fe}_3\text{O}_4@\text{SiO}_2\text{-NH}_2\text{-VO}^{2+}$ and $\text{Fe}_3\text{O}_4@\text{SiO}_2\text{-NH}_2\text{-Cu}^{2+}$ was analyzed with XPS. As shown in Fig. 5a, the peaks with binding energy at 25.9, 103.4, 154.8, 285.3, 401.8, 522.1, 532.6 eV were distributed to O 2s, Si 2p, Si 2s, C 1s, N 1s, V 2p, O 1s, which affirmed that these catalysts were made up of C, O, Si, V, N in the survey scan of $\text{Fe}_3\text{O}_4@\text{SiO}_2\text{-NH}_2\text{-VO}^{2+}$. As reported by the literature, the broadening of the Fe 2p_{1/2} peak (~711 eV) and Fe 2p_{3/2} peak (~724 eV) on the high energy side was a characteristic of Fe^{2+} in Fe_3O_4 .³³ Fig. 5a showed that there were no peaks with BEs at ~724 and ~711 eV. Moreover, the binding energy of V 2p_{1/2} at 524.1 eV and V 2p_{3/2} at 516.7 eV identified that after VO^{2+} ion anchored $\text{Fe}_3\text{O}_4@\text{SiO}_2\text{-NH}_2$, the valence state of V was +4.³⁴ Based on the XPS analysis, VO^+ should be anchored on NH_2 by the coordination bonds. Similarly, the XPS spectrum of $\text{Fe}_3\text{O}_4@\text{SiO}_2\text{-NH}_2\text{-Cu}^{2+}$ also demonstrated that it was constitute of N, C, O, Si, and Cu. The existence of Cu^{2+} was characterized by a Cu 2p_{3/2} peak at 933.2 eV, Cu 2p_{1/2} peak at 954.5 eV together with a satellite peak at 943.3 eV.³⁵

The surface composition of final solids (a mixture of $\text{Fe}_3\text{O}_4@\text{SiO}_2\text{-NH}_2\text{-VO}^{2+}$ and $\text{Fe}_3\text{O}_4@\text{SiO}_2\text{-NH}_2\text{-Cu}^{2+}$) were analyzed with XPS. As shown in Fig. 5e, the peaks with binding energy at 25.9, 103.4, 154.8, 285.3, 401.8, 522.1, 532.6, 933.2 eV were distributed to V 2p, N 1s, C 1s, Si 2s, Si 2p, O 2s, O 1s, Cu 2p, which affirmed that these catalysts were made up of C, O, Si, V, N, Cu in the survey scan of spent catalysts. However, the peaks with binding energy at 711, 724 eV were distributed to Fe 2p_{1/2}, Fe 2p_{3/2}, which also affirmed that the spent catalysts were composed of Fe, this probably due to a little Fe_3O_4 anchored the surface of the spent catalysts.

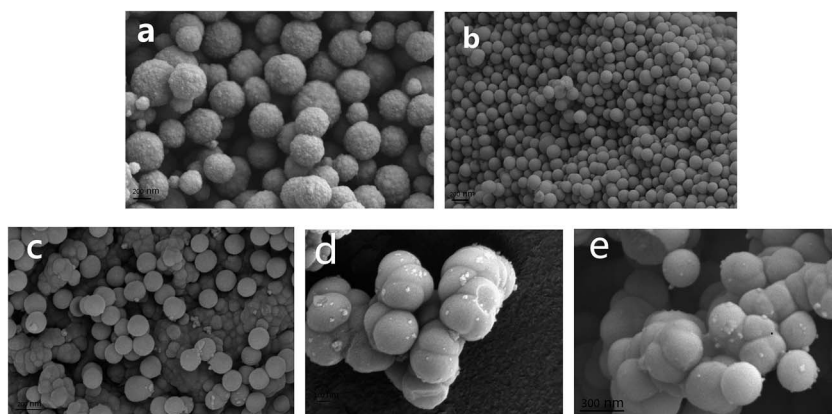


Fig. 2 SEM images of (a) Fe_3O_4 ; (b) $\text{Fe}_3\text{O}_4@\text{SiO}_2$; (c) $\text{Fe}_3\text{O}_4@\text{SiO}_2\text{-NH}_2$; (d) $\text{Fe}_3\text{O}_4@\text{SiO}_2\text{-NH}_2\text{-VO}^{2+}$; (e) $\text{Fe}_3\text{O}_4@\text{SiO}_2\text{-NH}_2\text{-Cu}^{2+}$.

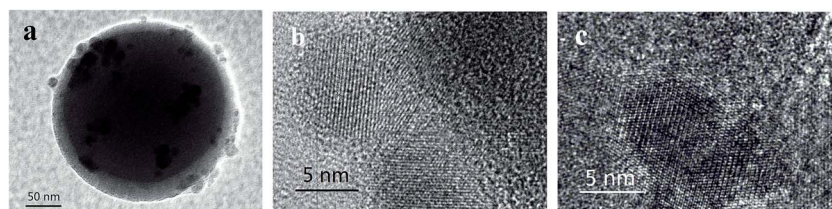


Fig. 3 TEM image of a typical core-shell structure (a); the lattice fringe of Cu^{2+} (b) and VO^{2+} (c).

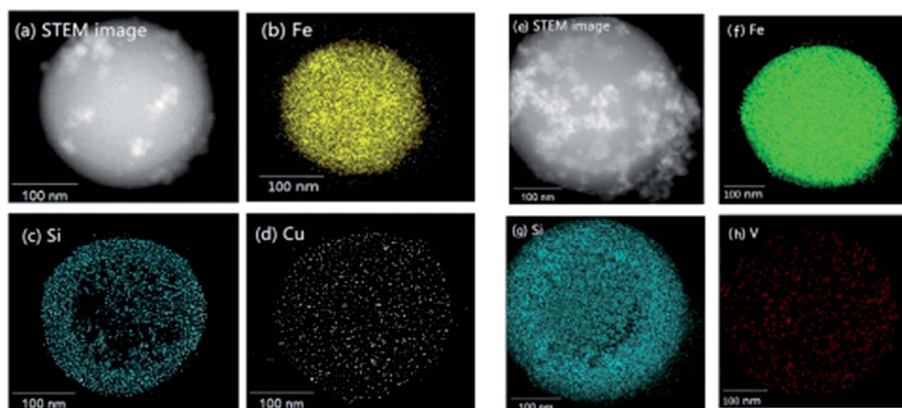


Fig. 4 (a) STEM image of Fe₃O₄@SiO₂-NH₂-Cu²⁺ and its corresponding EDX mapping images of (b) Fe, (c) Si, (d) Cu, (e) STEM image of Fe₃O₄@SiO₂-NH₂-VO²⁺ and its corresponding EDX mapping images of (f) Fe, (g) Si, (h) V.

In addition, as shown in Fig. 5f, the binding energy of V 2p_{1/2} at 524.1 eV and V 2p_{3/2} at 516.7 eV identified that after VO²⁺ ion anchored Fe₃O₄@SiO₂-NH₂, the valence state of V was +4. Meanwhile, the binding energy of Cu 2p_{3/2} at peak at 933.2 eV, and Cu 2p_{1/2} peak at 954.5 eV, which means the valence state of V was +2.³⁵ After the reaction, Cu and V amounts in the solution were determined by atomic absorption spectroscopy measurements, and the content of Cu and V were less than 0.005 g L⁻¹ and 0.5 g L⁻¹, respectively, which confirms the stability of final solids.

FT-IR technology was used to further characterized Fe₃O₄@SiO₂-NH₂, Fe₃O₄@SiO₂-NH₂-Cu²⁺ and Fe₃O₄@SiO₂-NH₂-VO²⁺. As shown in Fig. 6, there was no apparent difference among the three samples. A broad band at 1630 cm⁻¹ was presented in the spectra of Fe₃O₄@SiO₂-NH₂, Fe₃O₄@SiO₂-NH₂-Cu²⁺ and Fe₃O₄@SiO₂-NH₂-VO²⁺, which is attributed to the vibration of O-H bands in the silanol group and physically adsorbed water.³⁶ Besides, the spectra of the two catalysts contained the Si-O-Si bands at 1000–1200 cm⁻¹, which was distributed to the antisymmetric Si-O-Si stretching vibration. Meanwhile, a band at 582 cm⁻¹ was also observed in the catalysts, indicating the presence of Fe-O vibrations.³⁷ The aliphatic CH vibration associated with bands around 2920 cm⁻¹ are observed in the two catalysts as well, owing to the grafting APTES on the silica surface. In addition, an absorption band at 1558 cm⁻¹, which probably overlapped with the bending vibration of the adsorbed H₂O, was the NH bending vibration of the amine groups. As a result, the FT-IR technology results also identified that propyl amine groups were well anchored to the surface of Fe₃O₄@SiO₂.

The magnetic property of the binary catalysts was investigated by the PPMS with VSM option. Magnetic characterization using a magnetometer at 300 K indicates that the magnetization saturation values for Fe₃O₄, Fe₃O₄@SiO₂-NH₂-Cu²⁺ and Fe₃O₄@SiO₂-NH₂-VO²⁺ microspheres are 45, 30, and 29 emu g⁻¹ (Fig. 7), respectively. Besides, there was no remanence or coercivity for all of the above samples. As a result of high magnetization, the Fe₃O₄@SiO₂-NH₂-Cu²⁺ and Fe₃O₄@SiO₂-NH₂-VO²⁺ microspheres show fast response to the external magnet and

can be readily separated from the dispersion in less than 30 second (Scheme 4), which makes them favorable in diverse applications.

In order to study the surface area and porous nature of the materials, the N₂ adsorption-desorption isotherms of Fe₃O₄@SiO₂, Fe₃O₄@SiO₂-NH₂, Fe₃O₄@SiO₂-NH₂-Cu²⁺ and Fe₃O₄@SiO₂-NH₂-VO²⁺ were conducted. A typical isotherm of the four samples are shown in Fig. 8. Isotherms of these samples showed a type IV isotherm, and the samples were microporous material. With the loading of VO²⁺ and Cu²⁺, the hysteresis loop became shorter, corresponding to a reduction of the pore volume. Table 1 shows values of the BET surface area, pore size, and pore volume for Fe₃O₄@SiO₂, Fe₃O₄@SiO₂-NH₂, Fe₃O₄@SiO₂-NH₂-Cu²⁺ and Fe₃O₄@SiO₂-NH₂-VO²⁺. It was noted that Fe₃O₄@SiO₂ had much higher surface area and pore volume than other three samples. This seems logical as the loading of Cu²⁺ and VO²⁺ were dispersed and deposited on the surface of Fe₃O₄@SiO₂-NH₂, decreasing the pore diameter and thus diminishing the surface area.

The thermogravimetric analysis of the catalysts was conducted. As indicated in Fig. 9, the fresh catalyst Fe₃O₄@SiO₂-NH₂-Cu²⁺ and Fe₃O₄@SiO₂-NH₂-VO²⁺ absorbed more water than the spent catalysts because more weight loss of the former two samples from around 26 °C to 200 °C was observed compared to the spent catalysts, which probably owing to the relatively high the specific surface of the fresh catalysts. However, during 200–890 °C, the mass loss of three samples are 5.77%, 4.46% and 7.74%, respectively, which means the spent catalysts have higher mass loss than other two samples, which probably because the spent catalysts have absorbed more organic products on the surface. The thermal decomposition behavior of three samples by using differential scanning calorimetry (DSC) and the results was showed in Fig. 9 red line. It could be found that both heat-absorbing and heat-losing were exist before and after the reaction process. According to the DSC results, the endothermic reaction was the main reaction at low temperature and the exothermic reaction was predominant process at higher temperature.

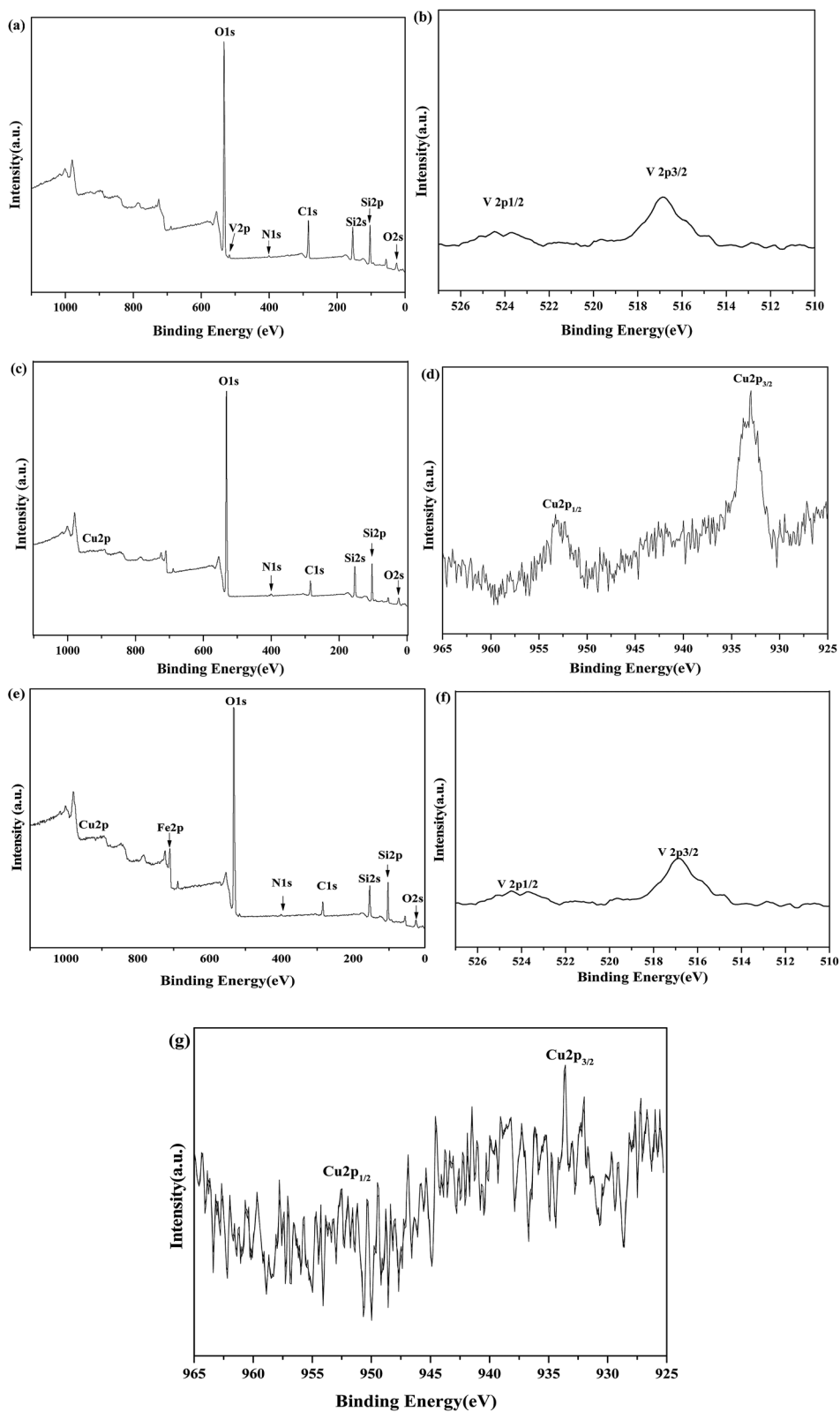


Fig. 5 The XPS spectra of the fresh samples and final solids samples. (a) Survey scan of $\text{Fe}_3\text{O}_4@ \text{SiO}_2\text{-NH}_2\text{-VO}^{2+}$; (b) high resolution XPS spectra of V $2p_{1/2}$; (c) survey scan of $\text{Fe}_3\text{O}_4@ \text{SiO}_2\text{-NH}_2\text{-Cu}^{2+}$; (d) high resolution XPS spectra of Cu 2p; (e) survey scan of final solid samples; (f) high resolution XPS spectra of V $2p_{1/2}$; (g) high resolution XPS spectra of Cu 2p.

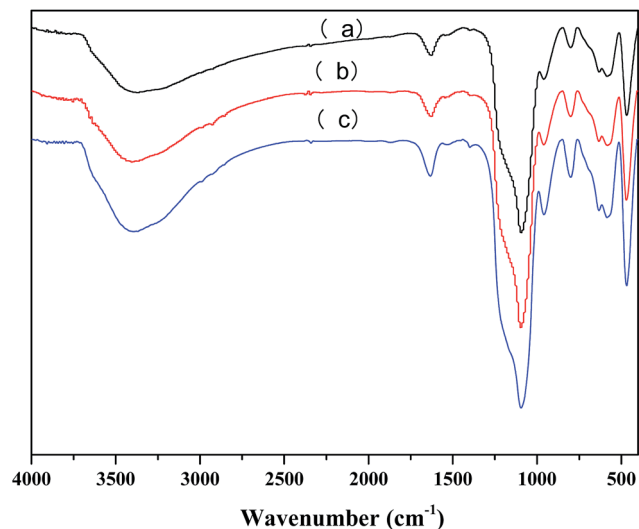


Fig. 6 FT-IR spectra of the three samples. (a) $\text{Fe}_3\text{O}_4@\text{SiO}_2\text{-NH}_2$; (b) $\text{Fe}_3\text{O}_4@\text{SiO}_2\text{-NH}_2\text{-Cu}^{2+}$; (c) $\text{Fe}_3\text{O}_4@\text{SiO}_2\text{-NH}_2\text{-VO}^{2+}$.

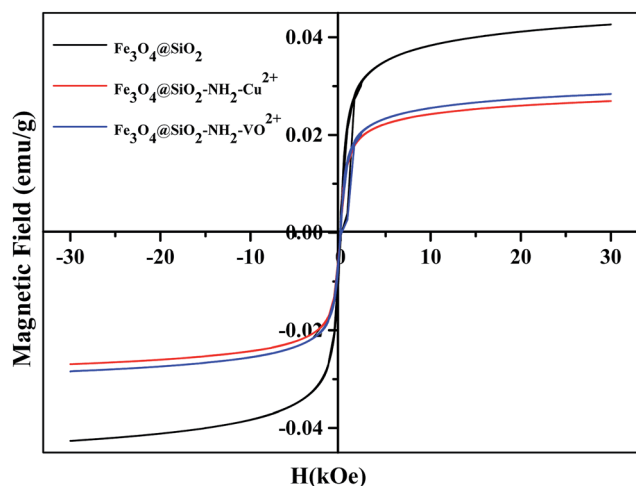


Fig. 7 Hysteresis loops of Fe_3O_4 , $\text{Fe}_3\text{O}_4@\text{SiO}_2\text{-NH}_2\text{-Cu}^{2+}$ and $\text{Fe}_3\text{O}_4@\text{SiO}_2\text{-NH}_2\text{-VO}^{2+}$ at 300 K.

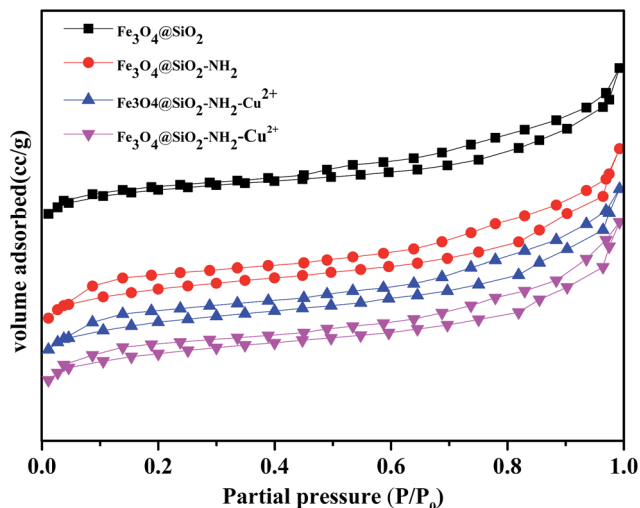


Fig. 8 Adsorption isotherms of $\text{Fe}_3\text{O}_4@\text{SiO}_2$; $\text{Fe}_3\text{O}_4@\text{SiO}_2\text{-NH}_2$; $\text{Fe}_3\text{O}_4@\text{SiO}_2\text{-NH}_2\text{-Cu}^{2+}$; $\text{Fe}_3\text{O}_4@\text{SiO}_2\text{-NH}_2\text{-VO}^{2+}$.

Table 1 Textural property of the four samples

Sample	Surface area ($\text{m}^2 \text{g}^{-1}$)	Pore volume ($\text{cm}^3 \text{g}^{-1}$)	Pore size (nm)
$\text{Fe}_3\text{O}_4@\text{SiO}_2$	192.592	0.172	3.58
$\text{Fe}_3\text{O}_4@\text{SiO}_2\text{-NH}_2$	151.699	0.170	4.48
$\text{Fe}_3\text{O}_4@\text{SiO}_2\text{-NH}_2\text{-Cu}^{2+}$	135.775	0.159	4.69
$\text{Fe}_3\text{O}_4@\text{SiO}_2\text{-NH}_2\text{-VO}^{2+}$	143.665	0.161	4.47

3.2. Catalytic oxidation of HMF over co-catalysts

The catalysts were investigated for the oxidation of 0.8 mmol HMF in 40 mL toluene by the autoclave reactor at 0.28 MPa O_2 pressure and 110 °C. The results runs after 1 h (high HMF conversion) can be seen in the Table 3. In the presence of $\text{Fe}_3\text{O}_4@\text{SiO}_2\text{-NH}_2\text{-VO}^{2+}$ catalyst alone, a conversion of HMF was obtained at 70.6% after 1 h. The major oxidation product was DFF, which gained a selectivity of 51.3%, while the yield was relatively lower at 36.2% (Table 3, entry 1). The HMF conversion was 21.0% with the single catalyst $\text{Fe}_3\text{O}_4@\text{SiO}_2\text{-NH}_2\text{-Cu}^{2+}$ (Table 3, entry 2). As previously reported by Ma *et al.*, "the use of



Scheme 4 The schematic illustration of procedures for recycling of catalysts and solvent.

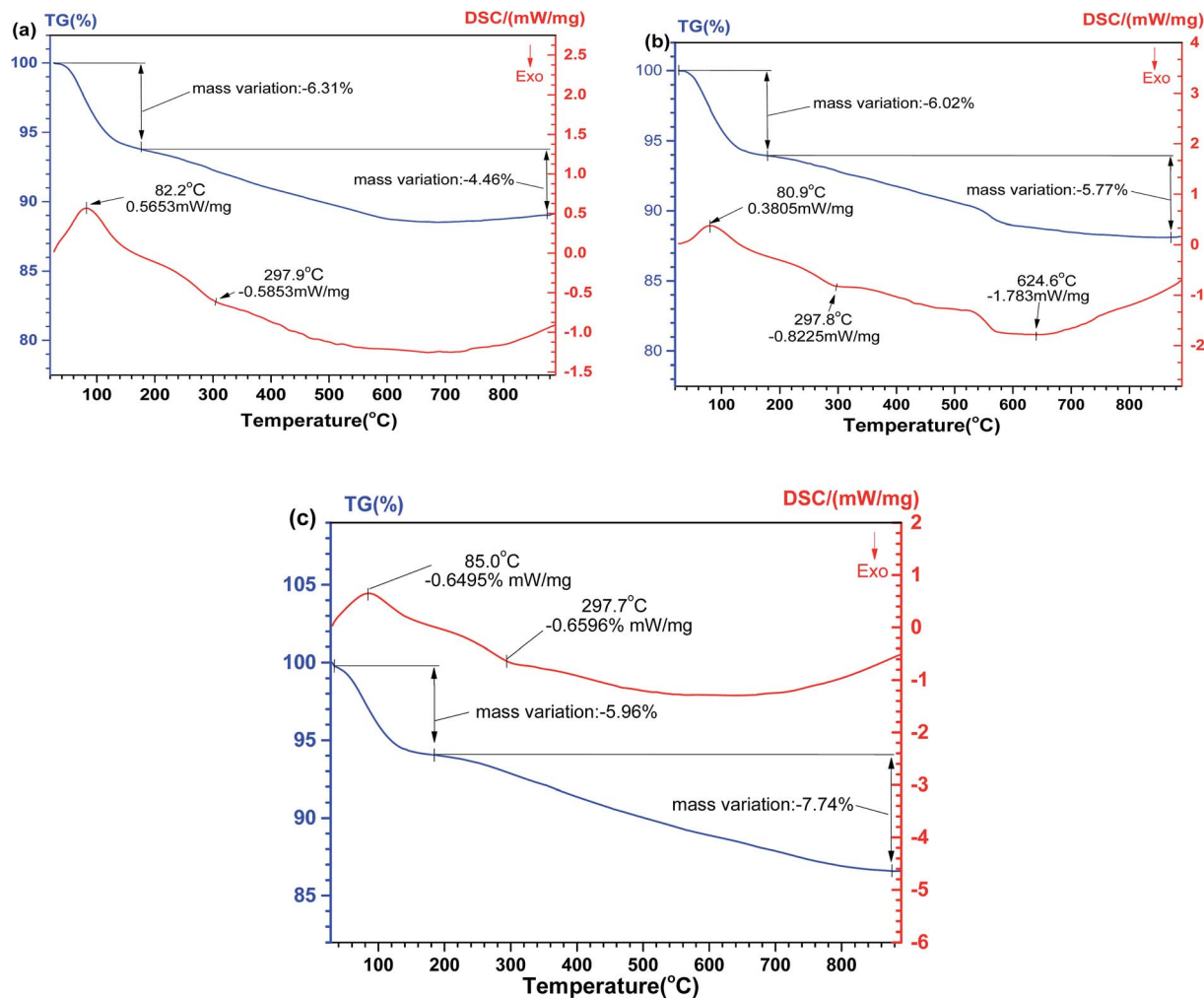


Fig. 9 TGA/DSC profiles for $\text{Fe}_3\text{O}_4@\text{SiO}_2\text{-NH}_2\text{-Cu}^{2+}$ (a), $\text{Fe}_3\text{O}_4@\text{SiO}_2\text{-NH}_2\text{-VO}^{2+}$ (b), and the final solids (c).

homogeneous $\text{VO}(\text{SO}_4)_2$ and $\text{Cu}(\text{NO}_3)_2$ indicated a synergic effect on oxidizing HMF into DFF.¹⁷ Hence, $\text{Fe}_3\text{O}_4@\text{SiO}_2\text{-NH}_2\text{-VO}^{2+}$ and $\text{Fe}_3\text{O}_4@\text{SiO}_2\text{-NH}_2\text{-Cu}^{2+}$ were used as the co-catalysts for the HMF oxidation. For purpose of giving more insights into the role that $\text{Fe}_3\text{O}_4@\text{SiO}_2\text{-NH}_2\text{-Cu}^{2+}$ played in the whole oxidation reaction, the amount of $\text{Fe}_3\text{O}_4@\text{SiO}_2\text{-NH}_2\text{-VO}^{2+}$ was designed at a constant, while the amount of $\text{Fe}_3\text{O}_4@\text{SiO}_2\text{-NH}_2\text{-Cu}^{2+}$ varied from 0 to 40 mg (Table 2, entries 3–5). As shown in Table 2, the conversion of HMF went up gradually with the increase of $\text{Fe}_3\text{O}_4@\text{SiO}_2\text{-NH}_2\text{-Cu}^{2+}$. Nearly quantitative HMF conversion was achieved *via* using 100 mg of $\text{Fe}_3\text{O}_4@\text{SiO}_2\text{-NH}_2\text{-VO}^{2+}$ and 30 mg of $\text{Fe}_3\text{O}_4@\text{SiO}_2\text{-NH}_2\text{-Cu}^{2+}$. Nevertheless, the DFF selectivity was not increased distinctly. The single catalyst $\text{Fe}_3\text{O}_4@\text{SiO}_2\text{-NH}_2\text{-VO}^{2+}$ alone gave DFF a selectivity of 70.6%, while the selectivity was promoted to 87.4% by the use of $\text{Fe}_3\text{O}_4@\text{SiO}_2\text{-NH}_2\text{-VO}^{2+}$ (100 mg) and $\text{Fe}_3\text{O}_4@\text{SiO}_2\text{-NH}_2\text{-Cu}^{2+}$ (30 mg) (Table 2, entry 5). These comparative results definitely showed that the presence of the two Cu^{2+} and VO^{2+} ion performs better catalytic effect than the individual counterparts on selective oxidizing HMF into DFF. Whereas, increasing the amount of $\text{Fe}_3\text{O}_4@\text{SiO}_2\text{-NH}_2\text{-Cu}^{2+}$ up to 40 mg, the results almost remained the same (Table 2, entries 5 *vs.* 6). Consequently, it should be noted

that the combined use of the co-catalysts performed the best catalytic performance on the HMF oxidation.

Since the reaction of oxidizing HMF over vanadium based catalysts were usually through the cycle between V^{4+} and V^{5+} , adding $\text{Fe}_3\text{O}_4@\text{SiO}_2\text{-NH}_2\text{-Cu}^{2+}$ could enhance the generation of active V^{5+} species to the promotion of HMF oxidation, which resembled the homogeneous $[\text{VO}(\text{SO}_4)_2\text{-Cu}(\text{NO}_3)_2]$.¹⁷ At the same time, the reduction Cu^+ can be easily reoxidized to Cu^{2+} through the oxygen molecule. Hence the whole catalytic recycle was completed.

Moreover, two groups of blank reactions were also conducted with Fe_3O_4 and $\text{Fe}_3\text{O}_4@\text{SiO}_2\text{-NH}_2$, respectively. In the two cases, mere oxidation products were detected by HPLC and HMF was nearly quantitatively recovered, which means VO^{2+} and Cu^{2+} ions are the active sites for the HMF oxidation reaction and HMF remained stable with no catalyst.

3.3. Catalytic oxidation of HMF in various solvents

To optimize the selectivity of DFF, the oxidation reaction was conducted in different solvents. The HMF conversion and the distribution of products were greatly influenced by the reaction

Table 2 Catalytic oxidation of HMF on various catalytic systems^a

Entry	Fe ₃ O ₄ @SiO ₂ -NH ₂ -VO ²⁺ amount (mg)	Fe ₃ O ₄ @SiO ₂ -NH ₂ -Cu ²⁺ amount (mg)	HMF conversion (%)	DFF yield (%)	DFF selectivity (%)
1	100	0	70.6	36.2	51.3
2	0	100	21.0	8.1	38.6
3	100	10	83.1	48.9	58.8
4	100	20	89.6	74.4	83.0
5	100	30	98.7	85.5	87.4
6	100	40	98.4	80.1	81.4
7	0	0	Trace	Trace	—

^a Reaction conditions: toluene (40 mL), HMF (100 mg, 0.8 mmol), 110 °C, O₂ (0.28 MPa), 1 h, 650 rpm.

Table 3 Effect of the reaction solvent on the aerobic oxidation of HMF into DFF^a

Entry	Solvent	HMF conversion (%)	DFF yield (%)	DFF selectivity (%)
1	Toluene	98.7	85.5	87.4
2	4-Chlorotoluene	98.6	84.6	86.8
3	Acetonitrile	75.0	35.5	47.3
4	MIBK	60.2	13.3	22.1
5	DMSO	13.8	1.4	10.1
6	H ₂ O	13.6	1.9	14.0
7	Toluene ^b	3.6	0.2	5.6

^a Reaction conditions: solvent (40 mL), HMF (100 mg, 0.8 mmol), 110 °C, O₂ (0.28 MPa), 1 h, 650 rpm, Fe₃O₄@SiO₂-NH₂-VO²⁺ (100 mg) and Fe₃O₄@SiO₂-NH₂-Cu²⁺ (30 mg). ^b Reaction conditions: solvent (40 mL), HMF (100 mg, 0.8 mmol), 110 °C, O₂ (0.28 MPa), 1 h, 650 rpm.

solvents. Generally, the best catalytic performance was obtained in aromatic solvents like 4-chlorotoluene and toluene (Table 3, entry 1–2), and the DFF selectivity were also highly achieved in the two solvents. Unlike in the aromatic solvents, the HMF conversions were much lower in other organic solvents like acetonitrile and MIBK (Table 3, entry 3–4), but the selectivity of products remained the same with no improvement. The lowest HMF conversion was observed in the strong organic solvent DMSO and deionized water. Based on the oxidation results in various solvents, the solvents showed a conspicuous influence on chemical reactions. However, the nature of the solvent effects is complex and the origin was still unclear.³⁸

In addition, the properties of the solvent, such as the polarity, acid–base properties, steric hindrance and dielectric constant, also have a great influence on the chemical reaction. Our catalytic system showed high HMF conversion in aromatic solvents, which might possibly due to the two reasons. On the one hand, since the catalyst surface was modified by an organic layer and the catalytic sites were located in organic layer, the aromatic solvents with relative low polarity as compared with toluene and 4-chlorotoluene would benefit to bring the substrate (HMF) to the catalytic sites, resulting in a higher catalytic activity. On the other hand, the solvents that contain heteroatoms (N, O) led to lower HMF conversions and DFF yields than aromatic solvents. The reason is probably the stronger interactions between the solvent (the heteroatoms N, O

as the electron donor) and the catalytic center. This phenomenon was also reported by Lignier *et al.* who used Au/TiO₂ for the oxidation of alcohols.³⁹ They found that solvents that did not contain heteroatoms (N, O, and S) resulted in significant product yields, which attributed to the stronger interaction between these solvents and the catalyst powder.

Finally, these results proved that the aromatic solvent was the excellent reaction medium for the HMF oxidation by using Fe₃O₄@SiO₂-NH₂-VO²⁺ (100 mg) and Fe₃O₄@SiO₂-NH₂-Cu²⁺ (30 mg) as the co-catalysts.

3.4. Effect of reaction time and temperature on aerobic oxidation of HMF into DFF

The reaction time played an important role for selective oxidation of HMF into DFF using Fe₃O₄@SiO₂-NH₂-VO²⁺ (100 mg) and Fe₃O₄@SiO₂-NH₂-Cu²⁺ (30 mg). The aerobic oxidation of HMF was conducted at 110 °C for 0.5, 1.0, 1.5, 2.0 h, respectively. As showed in Fig. 10, the HMF conversion was increased from 96.3% to 98.7% with the increase of reaction time from 0.5 to 1.0 h, followed by the HMF conversion almost remained

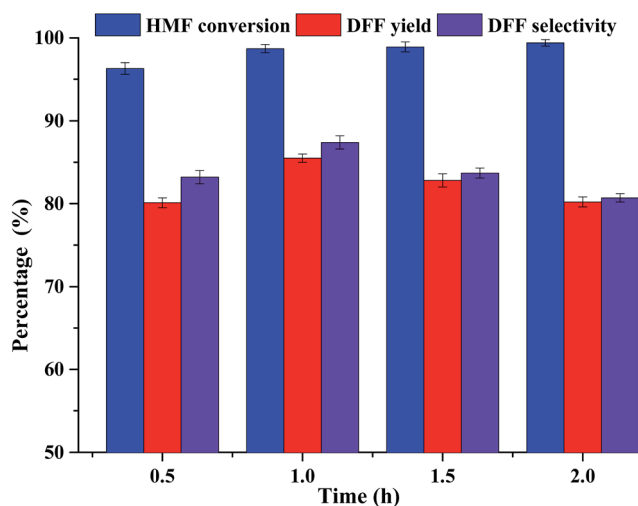


Fig. 10 The effect of the reaction time for the HMF oxidation. Reaction conditions: toluene (40 mL), HMF (100 mg, 0.8 mmol), 110 °C, O₂ (0.28 MPa), 650 rpm, Fe₃O₄@SiO₂-NH₂-VO²⁺ (100 mg) and Fe₃O₄@SiO₂-NH₂-Cu²⁺ (30 mg).

stable around 99.0% after 1.5 h. Meanwhile, the yield of DFF had witnessed a slightly growth from 0.5 to 1.0 h, in which the figure increased from 80.1% to its summit 85.5%, whereas what happened next was that it dropped back to 80.2% at 2.0 h, this is because as time increased, the generated DFF has been transferred into other oxidation products, such as 5-hydroxymethyl-2-furoic acid (HMFA) and 2,5-furandicarboxylic acid (FDCA), *etc.* Besides, a similar trend was observed for the selectivity of DFF.

The effectiveness of reaction temperature on the oxidizing HMF was investigated, and all the reactions were conducted at 130, 110, and 90 °C, respectively. The Fig. 11 showed that the HMF conversion would be increased with the increase of the reaction temperature was totally because raising the reaction temperature enhanced the movement of molecules, hence leading to the high reaction rate and the high HMF conversion. The conversion of HMF was 88.6% after reacting for 1 h at 90 °C with a DFF yield of 72.4%. Nevertheless, the HMF conversion increased up to 98.7% for reaction temperatures at 110 °C, and a corresponding yield of DFF was 85.5%. Further raising the temperature up to 130 °C, HMF obtained a conversion of 99.4%. However, the DFF yield was just 80.8%, which was a little lower than that gained at 110 °C. Similarly, it was also observed that the selectivity of DFF at 130 °C was also lower than those gained at 90 and 110 °C, respectively.

During the aerobic oxidation process, side reactions such as over-oxidizing HMF into HMFA could reduce the selectivity of DFF. For another, the substrate material HMF had poor stability at high temperature.³

3.5. Effect of O₂ pressure on aerobic oxidation of HMF into DFF

The effect of O₂ pressure on the oxidizing HMF was investigated and all the reactions were conducted at 0.28, 0.41, 0.55 and 0.69 MPa, respectively. Primarily, the oxidation reactions were

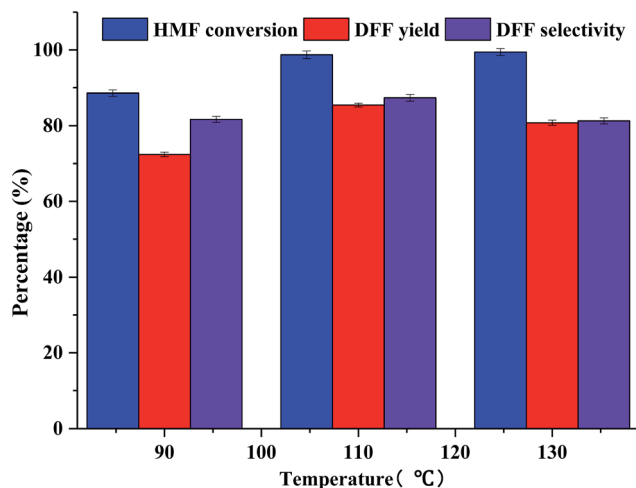


Fig. 11 The results of HMF oxidation at various reaction temperatures. Reaction conditions: toluene (40 mL), HMF (100 mg, 0.8 mmol), O₂ (0.28 MPa), 1 h, 650 rpm, Fe₃O₄@SiO₂-NH₂-VO²⁺ (100 mg) and Fe₃O₄@SiO₂-NH₂-Cu²⁺ (30 mg).

conducted with varying O₂ pressure, and higher O₂ pressure could raise the HMF conversion. Raising O₂ pressure from 0.28 MPa to 0.69 MPa, the HMF conversion increased from 98.7% to 99.4% under the same reaction conditions, whereas the selectivity of over-oxidized products (*e.g.* FFCA) were also increased (Fig. 12). Since the raised O₂ pressure conditions have contributed to the formation of the unexpected products, further reactions were carried out at 0.28 MPa of O₂ pressure.

3.6. Comparison of our method with other reported methods

The catalytic performance of VO²⁺/Cu²⁺ immobilized on Fe₃O₄@SiO₂-NH₂ catalyst was compared with that using other previously reported methods and the results are shown in Table 4. The heterogeneous Ru catalysts generally showed high HMF conversion and DFF yield (Table 4, entries 1–3), but some cases required high pressure (Table 4, entries 1–2), which was potentially dangerous in practical application. Non-noble based heterogeneous catalysts have also been reported for the oxidation of HMF. The vanadium based catalysts had some distinct drawbacks such as the requirement of high pressure, the need for a co-catalyst (Table 4, entry 4), and the loss of catalytic activity (Table 4, entry 5). Albeit our method showed a little lower DFF yield as compared with some of the above mentioned methods, it demonstrated a unique advantage (Table 4, entry 6). The VO²⁺/Cu²⁺ immobilized on Fe₃O₄@SiO₂-NH₂ catalyst could be readily separated from the reaction mixture by an external magnet.

3.7. Catalyst recycling experiments

Magnetic co-catalysts could be easily separated by an external magnet from the reaction mixture, which was significant for reusing the catalysts in view of green chemistry. For example, as shown in Scheme 3, the reaction mixture was much muddy after the oxidation reaction, but it shortly became clear with the help

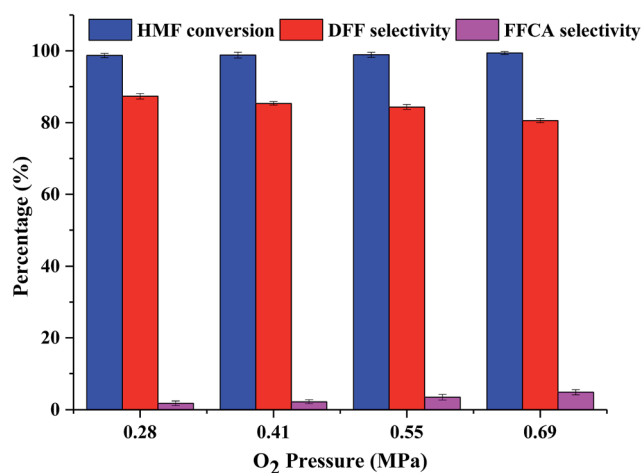


Fig. 12 The results of HMF oxidation under various O₂ pressure. Reaction conditions: toluene (40 mL), HMF (100 mg, 0.8 mmol), 110 °C, 1 h, 650 rpm, Fe₃O₄@SiO₂-NH₂-VO²⁺ (100 mg) and Fe₃O₄@SiO₂-NH₂-Cu²⁺ (30 mg).

Table 4 Catalytic oxidation of HMF into DFF using various methods

Entry	Catalyst	Reaction conditions	HMF conv (%)	DFF yield (%)	Ref.
1	Ru/C	383 K, 2.0 MPa of O ₂	100	96.0	15 and 40
2	Ru/γ-alumina	403 K, 40 psi O ₂	100	97.0	41
3	Fe ₃ O ₄ @SiO ₂ -NH ₂ -Ru(m)	393 K, 1 bar of O ₂ at 20 mL min ⁻¹	96.1	85.9	28
4	VO ²⁺ /Cu ²⁺ immobilized on sulfonated carbon catalyst	413, 40 bar of Ar	100	98.0	42
5	V ₂ O ₅ /H-beta	398 K, 10 bar of O ₂	84.8	84.0	43
6	VO ²⁺ /Cu ²⁺ immobilized on Fe ₃ O ₄ @SiO ₂ -NH ₂ catalyst	383 K, 0.28 MPa of O ₂	98.7	85.5	This work

of an external magnet. Thereafter the catalysts were well separated by decantation from the reaction mixture. The solvent toluene was collected by distilling from the mixture under a reduced O₂ pressure, keeping the major product DFF in the residue. Since oxidation products (*i.e.* HMFCa, DFF, and FDCA) are quite different in structure, the polarity of DFF is much lower than that of FDCA and HMFCa. Therefore, once the mixture was separated on a silica gel, DFF would firstly be washed off from the elution of solvent owing to its short retention time on silical gel. The recycled catalysts and toluene would be reused for several cycles.

The recycle of co-catalysts was carried out, and the aerobic oxidizing HMF into DFF was regarded as a model reaction. All the reactions were conducted at 110 °C under 0.28 MPa with 100 mg of Fe₃O₄@SiO₂-NH₂-VO²⁺ and 30 mg of Fe₃O₄@SiO₂-NH₂-Cu²⁺ for 1.0 h. The reused catalysts were washed by ethanol and toluene to eliminate the adsorbed products, followed by being dried at 60 °C in a vacuum oven overnight. Then the reused catalysts were used for the next cycle under same reaction conditions. As shown in Fig. 13, the DFF yield almost remained the same (85.5% in the first run *versus* 81.2% in the fourth run), which indicated that the catalysts could be used again with no obvious loss of catalytic activity. Albeit non-magnetic heterogeneous catalysts could also be recycled, the conventional

methods (*e.g.* filtration and centrifugation) made an unavoidable loss of active site during the catalysts recycling.⁴⁴ However, separating the catalysts by an external magnet will undoubtedly avoid the loss of catalysts during the recycling process.

4. Conclusion

In summary, amino-functionalized Fe₃O₄@SiO₂ (Fe₃O₄@SiO₂-NH₂) was prepared and used as a proper support for the immobilization of catalytic Cu²⁺ and VO²⁺ ions.

Fe₃O₄@SiO₂-NH₂-VO²⁺ and Fe₃O₄@SiO₂-NH₂-Cu²⁺ were applied to the aerobic oxidation of HMF into DFF with a HMF conversion of 98.7%. The catalytic performance was greatly influenced by the reaction solvents, probably relating with the solvent polarity and acid–base of the solvent. In addition, the catalysts would be successfully separated by an external magnet from the reaction mixture, and could be reused for several times with no loss of catalytic activity. The high activity, magnetic recyclability and stability make them promising applications in the conversion of biomass-derived platform chemicals into more valuable bulk chemicals.

Acknowledgements

This work was supported by Science and Technology Program of Guangzhou (201607020025), Fundamental Research Funds for the Central Universities (201522124) and Guangdong Natural Science Foundation (2016A030313489).

References

- 1 J. C. Serrano-Ruiz and J. A. Dumesic, Catalytic routes for the conversion of biomass into liquid hydrocarbon transportation fuels, *Energy Environ. Sci.*, 2011, **4**, 83–99.
- 2 L. Hu, G. Zhao, W. Hao, X. Tang, Y. Sun, L. Lin and S. Liu, Catalytic conversion of biomass-derived carbohydrates into fuels and chemicals *via* furanic aldehydes, *RSC Adv.*, 2012, **2**, 11184–11206.
- 3 M. J. Climent, A. Corma and S. Iborra, Conversion of biomass platform molecules into fuel additives and liquid hydrocarbon fuels, *Green Chem.*, 2014, **16**, 516–547.
- 4 B. Liu, Z. H. Zhang, K. C. Huang and Z. F. Fang, Efficient conversion of carbohydrates into 5-ethoxymethylfurfural in ethanol catalyzed by AlCl₃, *Fuel*, 2013, **113**, 625–631.

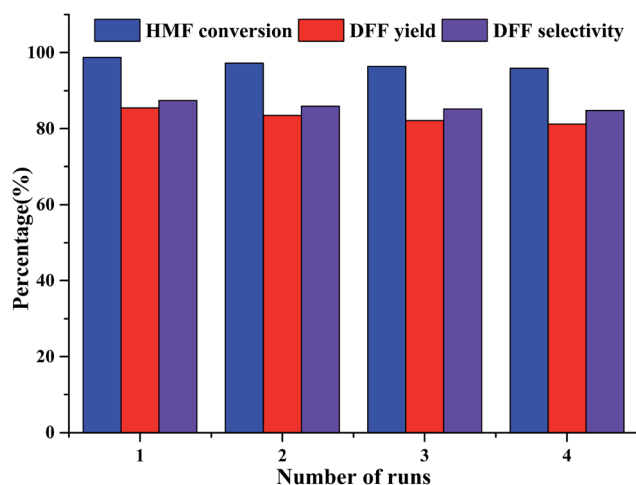


Fig. 13 The results of catalysts recycle. Reaction conditions: HMF (100 mg, 0.8 mmol), toluene (40 mL), 110 °C, O₂ (0.28 MPa), 1 h, 650 rpm, Fe₃O₄@SiO₂-NH₂-VO²⁺ (100 mg) and Fe₃O₄@SiO₂-NH₂-Cu²⁺ (30 mg).

- 5 D. Fouquet and T. B. Johansson, European renewable energy policy at crossroads-focus on electricity support mechanisms [J], *Energy policy*, 2008, **36**(11), 4079–4092.
- 6 R. J. van Putten, J. C. van der Waal, E. de Jong, C. B. Rasrendra, H. J. Heeres and J. G. de Vries, *Chem. Rev.*, 2013, **113**, 1499–1597.
- 7 R. Alamillo, M. Tucker, M. Chia, *et al.*, The selective hydrogenation of biomass-derived 5-hydroxymethylfurfural using heterogeneous catalysts[J], *Green Chem.*, 2012, **14**(5), 1413–1419.
- 8 Z. Du, J. Ma, F. Wang, *et al.*, Oxidation of 5-hydroxymethylfurfural to maleic anhydride with molecular oxygen[J], *Green Chem.*, 2011, **13**(3), 554–557.
- 9 A. Gandini and N. M. Belgacem, Recent advances in the elaboration of polymeric materials derived from biomass components [J], *Polymer Int.*, 1998, **47**(3), 267–276.
- 10 M. del Poeta, W. A. Schell, C. C. Dykstra, S. Jones, R. R. Tidwell, A. Czarny, M. Bajic, A. Kumar, D. Boykin and J. R. Perfect, *Antimicrob. Agents Chemother.*, 1998, **42**, 2495.
- 11 K. T. Hopkins, W. D. Wilson, B. C. Bendan, D. R. McCurdy, J. E. Hall, R. R. Tidwell, A. Kumar, M. Bajic and D. W. Boykin, *J. Med. Chem.*, 1998, **41**, 3872.
- 12 A. S. Amarasekara, D. Green and L. T. D. Williams, Renewable resources based polymers: synthesis and characterization of 2,5-diformylfuran-urea resin [J], *Eur. Polym. J.*, 2009, **45**(2), 595–598.
- 13 K. Weissermel and H. J. Arpe, *Industrial Organic Chemistry*, VC-Wiley, Weinheim, 1997, p. 225.
- 14 W. Partenheimer and V. V. Grushin, *Adv. Synth. Catal.*, 2001, **343**, 102–111.
- 15 J. Nie and H. Liu, Efficient aerobic oxidation of 5-hydroxymethylfurfural to 2,5-diformylfuran on manganese oxide catalysts [J], *J. Catal.*, 2014, **316**, 57–66.
- 16 G. D. Yadav and R. V. Sharma, Biomass derived chemicals: environmentally benign process for oxidation of 5-hydroxymethylfurfural to 2,5-diformylfuran by using Nano-fibrous Ag-OMS-2-catalyst [J], *Appl. Catal., B*, 2014, **147**, 293–301.
- 17 J. Ma, Z. Du, J. Xu, Q. Chu and Y. Pang, Efficient aerobic oxidation of 5-hydroxymethylfurfural to 2,5-diformylfuran, and synthesis of a fluorescent material, *ChemSusChem*, 2011, **4**, 51–54.
- 18 E. Rafiee and S. Eavani, $\text{H}_3\text{PW}_{12}\text{O}_{40}$ supported on silica-encapsulated $\gamma\text{-Fe}_2\text{O}_3$ nanoparticles: a novel magnetically-recoverable catalyst for three-component Mannich-type reactions in water [J], *Green Chem.*, 2011, **13**(8), 2116–2122.
- 19 M. Masteri-Farahani, J. Movassagh, F. Taghavi, *et al.*, Magnetite-polyoxometalate hybrid nanomaterials: synthesis and characterization [J], *Chem. Eng. J.*, 2012, **184**, 342–346.
- 20 W. Li, Y. H. Deng, Z. X. Wu, X. F. Qian, J. P. Yang, Y. Wang, D. Gu, F. Zhang, B. Tu and D. Y. Zhao, *J. Am. Chem. Soc.*, 2011, **133**, 15830.
- 21 W. R. Zhao, J. L. Gu, L. X. Zhang, H. R. Chen and J. L. Shi, *J. Am. Chem. Soc.*, 2005, **127**, 8916.
- 22 Y. G. Wang, Y. R. Wang, E. J. Hosono, K. X. Wang and H. S. Zhou, *Angew. Chem., Int. Ed.*, 2008, **4**(7), 7461.
- 23 Y. Deng, D. Qi, C. Deng, *et al.*, Superparamagnetic high-magnetization microspheres with an $\text{Fe}_3\text{O}_4@\text{SiO}_2$ core and perpendicularly aligned mesoporous SiO_2 shell for removal of microcystins [J], *J. Am. Chem. Soc.*, 2008, **130**(1), 28–29.
- 24 Y. Deng, Y. Cai, Z. Sun, *et al.*, Multifunctional mesoporous composite microspheres with well-designed nanostructure: a highly integrated catalyst system [J], *J. Am. Chem. Soc.*, 2010, **132**(24), 8466–8473.
- 25 N. Ren, A. G. Dong, W. B. Cai, Y. H. Zhang, W. L. Yang, S. J. Huo, Y. Chen, S. H. Xie, Z. Gao and Y. Tang, *J. Mater. Chem.*, 2004, **14**, 3548.
- 26 T. Yokoi, T. Tatsumi and H. Yoshitake, Fe^{3+} coordinated to amino-functionalized MCM-41: an adsorbent for the toxic oxyanions with high capacity, resistibility to inhibiting anions, and reusability after a simple treatment [J], *J. Colloid Interface Sci.*, 2004, **274**(2), 451–457.
- 27 A. S. M. Chong and X. S. Zhao, Functionalized nanoporous silicas for the immobilization of penicillin acylase [J], *Appl. Surf. Sci.*, 2004, **237**(1), 398–404.
- 28 S. Wang, Z. Zhang, L. Bing, *et al.*, Environmentally friendly oxidation of biomass derived 5-hydroxymethylfurfural into 2,5-diformylfuran catalyzed by magnetic separation of ruthenium catalyst, *Ind. Eng. Chem. Res.*, 2014, **53**(14), 5820–5827.
- 29 X. Liu, J. Xiao, H. Ding, *et al.*, Catalytic aerobic oxidation of 5-hydroxymethylfurfural over VO^{2+} and Cu^{2+} immobilized on amino functionalized SBA-15[J], *Chem. Eng. J.*, 2016, **283**, 1315–1321.
- 30 S. G. Wang, Z. H. Zhang, B. Liu and J. L. Li, Silica coated magnetic Fe_3O_4 nanoparticles supported phosphotungstic acid: a novel environment-friendly catalyst for the synthesis of 5-ethoxymethylfurfural from 5-hydroxymethylfurfural and fructose, *Catal. Sci. Technol.*, 2013, **3**, 2104–2112.
- 31 J. Lee, Y. Lee, J. K. Youn, H. B. Na, T. Yu, H. Kim, S. M. Lee, Y. M. Koo, J. H. Kwak, H. G. Park, H. N. M. Hwang, J. G. Park, J. Kim and T. Hyeon, Simple synthesis of functionalized superparamagnetic magnetite/silica core/shell nanoparticles and their application as magnetically separable high-performance biocatalysts, *Small*, 2008, **4**, 143–152.
- 32 G. P. Rachiero, U. B. Demirci and P. Miele, Facile synthesis by polyol method of a ruthenium catalyst supported on $\gamma\text{-Al}_2\text{O}_3$ for hydrolytic dehydrogenation of ammonia borane, *Catal. Today*, 2011, **170**, 85–92.
- 33 G. Kataby, A. Ulman, M. Cojocarua and A. Gedanken, Coating a bola-amphiphile on amorphous iron nanoparticles, *J. Mater. Chem.*, 1999, **9**, 1501–1506.
- 34 A. S. Ogunlaja, S. Khene, E. Antunes, T. Nyokong, N. Torto and Z. R. Tshentu, The development of catalytic oxovanadium(IV)-containing microspheres for the oxidation of various organosulfur compounds, *Appl. Catal., A*, 2013, **462**, 157–167.
- 35 S. Poulston, P. M. Parlett, P. Stone and M. Bowker, Surface oxidation and reduction of CuO and Cu_2O studied using XPS and XAES, *Surf. Interface Anal.*, 1996, **24**, 811–820.

- 36 X. Wang, K. S. K. Lin, J. C. C. Chan and S. Cheng, Direct synthesis and catalytic applications of ordered large pore amino propyl-functionalized SBA-15 mesoporous materials, *J. Phys. Chem. B*, 2005, **109**, 1763–1769.
- 37 C. He, T. Sasaki, Y. Shimizu and N. Koshizaki, One-step synthesis of maghemite (γ -Fe₂O₃) nanoparticles by wet chemical method, *Appl. Surf. Sci.*, 2008, **254**, 2196–2202.
- 38 R. R. Sever and T. W. Root, DFT study of solvent coordination effects on titanium based epoxidation catalysts. Part one: formation of the titanium hydroperoxo intermediate, *J. Phys. Chem. B*, 2003, **107**, 4080–4089.
- 39 P. Lignier, S. Mangematin, F. Morfin, J. Rousset and V. Caps, Solvent and oxidant effects on the Au/TiO₂-catalyzed aerobic epoxidation of stilbene, *Catal. Today*, 2008, **138**, 50–54.
- 40 S. K. R. Patil and C. R. F. Lund, Formation and growth of humins *via* aldol addition and condensation during acid-catalyzed conversion of 5-hydroxymethylfurfural, *Energy Fuels*, 2011, **25**, 4745–4755.
- 41 C. A. Antonyraj, J. Jeong, B. Kim, S. Shin, S. Kim, K.-Y. Lee and J. K. Cho, Selective oxidation of HMF to DFF using Ru/ γ -alumina catalyst in moderate boiling solvents toward industrial production, *J. Ind. Eng. Chem.*, 2013, **19**, 1056–1059.
- 42 N.-T. Le, P. Lakshmanan, K. Cho, Y. Han and H. Kim, Selective oxidation of 5-hydroxymethyl-2-furfural into 2,5-diformylfuran over VO²⁺ and Cu²⁺ ions immobilized on sulfonated carbon catalysts, *Appl. Catal., A*, 2013, **464–465**, 305–312.
- 43 I. Sadaba, Y. Y. Gorbaney, S. Kegnaes, S. S. R. Putluru, R. W. Berg and A. Riisager, Catalytic performance of zeolite-supported vanadia in the aerobic oxidation of 5-hydroxymethylfurfural to 2,5-diformylfuran, *ChemCatChem*, 2013, **5**, 284–293.
- 44 Y. Liu, L. Xu, B. B. Xu, Z. K. Li, L. P. Jia and W. H. Guo, Toluene alkylation with 1-octene over supported heteropoly acids on MCM-41 catalysts, *J. Mol. Catal. A: Chem.*, 2009, **297**, 86–92.